



Structural and optical characterization of $\text{Zn}_{0.95-x}\text{Mg}_{0.05}\text{Al}_x\text{O}$ nanoparticles

A.N. Mallika*, A.Ramachandra Reddy, K. Sowribabu, K.Venugopal Reddy

Department of Physics, Materials Science Laboratory, National Institute of Technology, Warangal 506004, Telangana, India

Received 11 November 2014; received in revised form 18 March 2015; accepted 18 March 2015

Available online 8 April 2015

Abstract

The structural and optical properties of ZnO nanoparticles doped simultaneously with Mg and Al were investigated. XRD results revealed the hexagonal wurtzite crystalline structure of ZnO. The FE-SEM study confirmed the formation of nano-sized homogeneous grains whose sizes decreased monotonously with increasing doping concentrations of Mg and Al. The absorption spectra showed that band gap increased from 3.20 to 3.31 eV with Mg doping. As the Al concentration changed from $x=0.01$ to $x=0.06$ mol% at constant Mg concentration the band gap observed to be decreased. Particle sizes estimated from effective mass approximation using absorption data and these values are in good agreement with the crystallite sizes calculated from XRD data. Raman spectra of ZnO showed a characteristic peak at 436 cm^{-1} correspond to a non-polar optical phonon E_2 (high). With increase of the Al doping concentrations, E_2 (high) phonon frequency shifted to 439 cm^{-1} from to 436 cm^{-1} . The origin of E_2 (high) peak shift in ZnO nanoparticles is attributed to optical phonon confinement effects or the presence of intrinsic defects on the nanoparticles. PL spectra indicated that with increase of Al co-doping along with Mg into ZnO, intensity of the peak positioned at 395 nm was initially increased at $x=0$ and then decreased with increase of the Al concentrations from $x=0.01$ to $x=0.06$ mol%.

© 2015 Elsevier Ltd and Techna Group S.r.l. All rights reserved.

Keywords: C. Optical properties; Nanostructures; Scanning electron microscopy (SEM); Crystal structure; Raman spectroscopy

1. Introduction

Among the wide band gap semiconductor materials, zinc oxide (ZnO) is one of the versatile and important materials that are being widely used in optoelectronic devices; it has a direct band gap of 3.37 eV at room temperature and exciton binding energy of 60 meV which is much higher than GaN (21 meV) [1]. Such remarkable property makes it a lucrative material for room temperature UV lasing devices and is thought to be one of the most promising candidates for applications in micro-electronic and optoelectronic devices. Apart from this, it is being used frequently in solar cells, transparent thin film transistors, ultraviolet (UV) photo-detectors, light emitting diodes (LEDs) and piezo-electric devices etc. [2]. Particularly, nanocrystals of ZnO show some fascinating properties like room temperature (RT) lasing in UV and visible regions. It is an interesting material from several points of view as well as it

is one of the few oxides that show quantum confinement effects in an experimentally accessible size range [3]. In addition to this, it is one of a select group of materials currently being considered to compete with tin doped indium oxide and tin oxide for applications including flat panel displays, solar cells, and energy efficient windows [4]. In order to enhance different properties of ZnO, many research groups have been extensively working by controlling: the doping concentrations, process parameters and annealing effects [5]. The materials with wide band gap and moderate electrical conductivity are useful as transparent electrodes in photovoltaic cells for improving the efficiency [6,7]. The band gap and electrical properties of ZnO nanoparticles can also be improved simultaneously by Mg and Al co-doping. Yao et al. have studied the influence of annealing temperature on the structural and optical properties of Al and Mg co-doped ZnO thin films [8]. Heiba et al. reported the structural and magnetic properties of nano-ZnO with (Al/Mg) co-doping [9]. With Al and K codoping the structural and optical properties of ZnO thin films was reported by Xu et al. [10]. Whereas, Arda et al. have reported the critical doping concentration of Al to get the

*Corresponding author.

E-mail addresses: mallika.nitw@gmail.com, mallika@nitw.ac.in (A.N. Mallika).

minimum line-width and maximum g -factor with Mg and Al codoping [11]. Recently, Bikowski et al. studied the role of grain barriers traps in polycrystalline and epitaxial magnetron-sputtered ZnO:Al and $Zn_{1-x}Mg_xO$:Al films [12]. Different chemical methods have been reported for the synthesis of ZnO nanoparticles like the sol–gel method [13], solo-chemical processes [14], precipitation [15], laser ablation method [16], dc thermal plasma synthesis [17], spray pyrolysis [18], pyrolysis [19], hydrothermal synthesis [20]. The sol–gel method is preferable among these due to low cost of the precursors and it provides good control over material composition at molecular level [21]. In the present study, Mg doping content of Mg–Al co-doped ZnO (AMZO) nanoparticles kept constant and Al concentrations varied. AMZO nanoparticles with different Al doping contents were synthesized by the sol–gel method. The main goal of this work is to investigate the influence of Al doping contents on Mg doped ZnO nanoparticles structure, surface morphology, optical band gap, and photoluminescence properties of ZnO nanoparticles.

2. Experimental procedure

Zinc nitrate hexahydrate ($Zn(NO_3)_2 \cdot 6H_2O$), Magnesium nitrate hexahydrate ($Mg(NO_3)_2 \cdot 6H_2O$), Aluminum nitrate hexahydrate ($Al(NO_3)_3 \cdot 9H_2O$) and PVA in suitable quantities were used for the synthesis of $Zn_{0.95-x}Mg_{0.05}Al_xO$ nanoparticles. The preparation of ZnO is same as the method described elsewhere [22]. One of these samples left undoped and in all the remaining samples, Magnesium concentration was fixed to 5 mole% and Aluminum concentrations were varied with $x=0, 0.01, 0.02$ and 0.06 mol% such that the stoichiometry $Zn_{0.95-x}Mg_{0.05}Al_xO$ was achieved. The samples were coded as pure (undoped), AMZ0 (with Al $x=0$), AMZ1 (with Al $x=0.01$), AMZ2 (with Al $x=0.02$) and AMZ6 (with Al $x=0.06$). The structure of the samples was studied by using PANalytical X'Pert3 powder diffractometer (XRD) equipped with $CuK\alpha$ radiation ($\lambda=1.5418 \text{ \AA}$). The morphology and grain size distribution of the samples were investigated using FE-SEM (Model: Carl Zeiss Ultra 55). Absorption spectra of the samples were acquired using a UV–visible spectrophotometer (Model: Varian, Cary 5000). Raman spectra of samples were recorded in the back scattering geometry at room temperature using Horiba-Jobin-Yvon LabRam HR high resolution micro-Raman spectrograph, with 514 nm of Argon ion laser as the excitation source. PL measurements were performed on a Jobin Yuon spectrofluorometer (Model: Fluorolog-FI3-11) equipped with a Xenon lamp of 450 W.

3. Results and discussion

3.1. X-ray studies

Fig. 1(a) shows the XRD patterns of Mg, Al co-doped ZnO nanoparticles. XRD patterns depicts the characteristic peaks corresponding to (100), (002), (101), (102), (110) and (103) reflection planes of wurtzite structure of ZnO [22]. No diffraction peaks due to Mg, Al, MgO, Al_2O_3 , or other impurity phases

were detected within the experimental limit. This finding indicated that Mg^{2+} and Al^{3+} ions were substituted into Zn^{2+} ion sites or incorporated into interstitial sites in the lattice without altering the hexagonal wurtzite structure of ZnO. From the XRD peaks, it is observed that, with reference to the pure ZnO diffraction peaks, Mg doping (AMZO) shifted the peaks to higher angles, suggesting that the unit cell expands to accommodate the Mg ions. This may be because of Mg ions preferring to occupy interstitial sites [23]. With Al co-doping, for AMZ1 sample, the peaks shifted to lower angles. With further increase of Al concentrations, for AMZ2 and AMZ6 samples, they shifted back to higher angles. The shift in these diffraction peaks can be described, primarily the lower angle shift is due to the fact that the ionic radii of Al^{3+} (0.39 \AA) which is lower than the ionic radii of Mg^{2+} (0.57 \AA) and Zn^{2+} (0.60 \AA). Therefore, it may try to occupy/replace the Zn lattice site. Further increase in the Al doping concentrations forces Al to occupy the interstitial sites, resulting peak broadening and higher angle shifts. The peak shift towards lower/higher 2θ value with respect to the bulk peak profiles have been attributed to compressive/tensile strain in the sample [24]. Therefore, the shift in these diffraction peaks is thus correlated to the strain produced and it may result to shift in the diffraction angles by changing inter planar spacing. However, there is reduction in the intensities of peaks with increase of Al concentrations in ZnO, which demonstrates the low crystal quality of doped ZnO nanostructures. The crystallite size d_{xrd} of the samples was calculated according to Scherrer's formula [25], using the parameters derived from the X-ray diffraction patterns. The average crystallite sizes calculated for all the samples are given in Table 1. The graph has been plotted between full width at half-maxima (FWHM) and crystallite sizes calculated from Scherrer's formula and shown in Fig. 1(b). In general, the FWHM is inversely proportional to the grain size [26], it is clearly observed in the Fig. 1(b) that, the FWHM increased with increasing dopant concentrations, thus, the increased FWHM refers to decrease in grain size which in turn indicates poor crystal quality of doped ZnO nanoparticles. In other words, at higher concentration of doping, it leads to degradation of the crystallinity which may be due to segregation of dopants in grain boundaries. At higher doping concentration, due to larger nuclear charge of Al^{3+} , extrinsic Al^{3+} will capture more oxygen in competition with Zn^{2+} which decreases the crystallinity and hexagonal structure of the nano-crystals [27]. The bond length (l) of Zn–O is calculated using the following equation [28]:

$$l = \sqrt{\left(\frac{a^2}{3} + \left(\frac{1}{2} - u\right)^2 c^2\right)}$$

where u is the positional parameter which can be expressed as $u = ((a^2/3c^2) + 0.25)$, [29]

$$a = \frac{\lambda}{\sqrt{3} \sin \theta}, \quad c = \frac{\lambda}{\sin \theta}.$$

The bond lengths calculated is tabulated and are initially decreased with Mg doping for AMZO sample. With Al co-doping along with Mg in to ZnO, at $x=0.01$ mole% (AMZ1) the bond

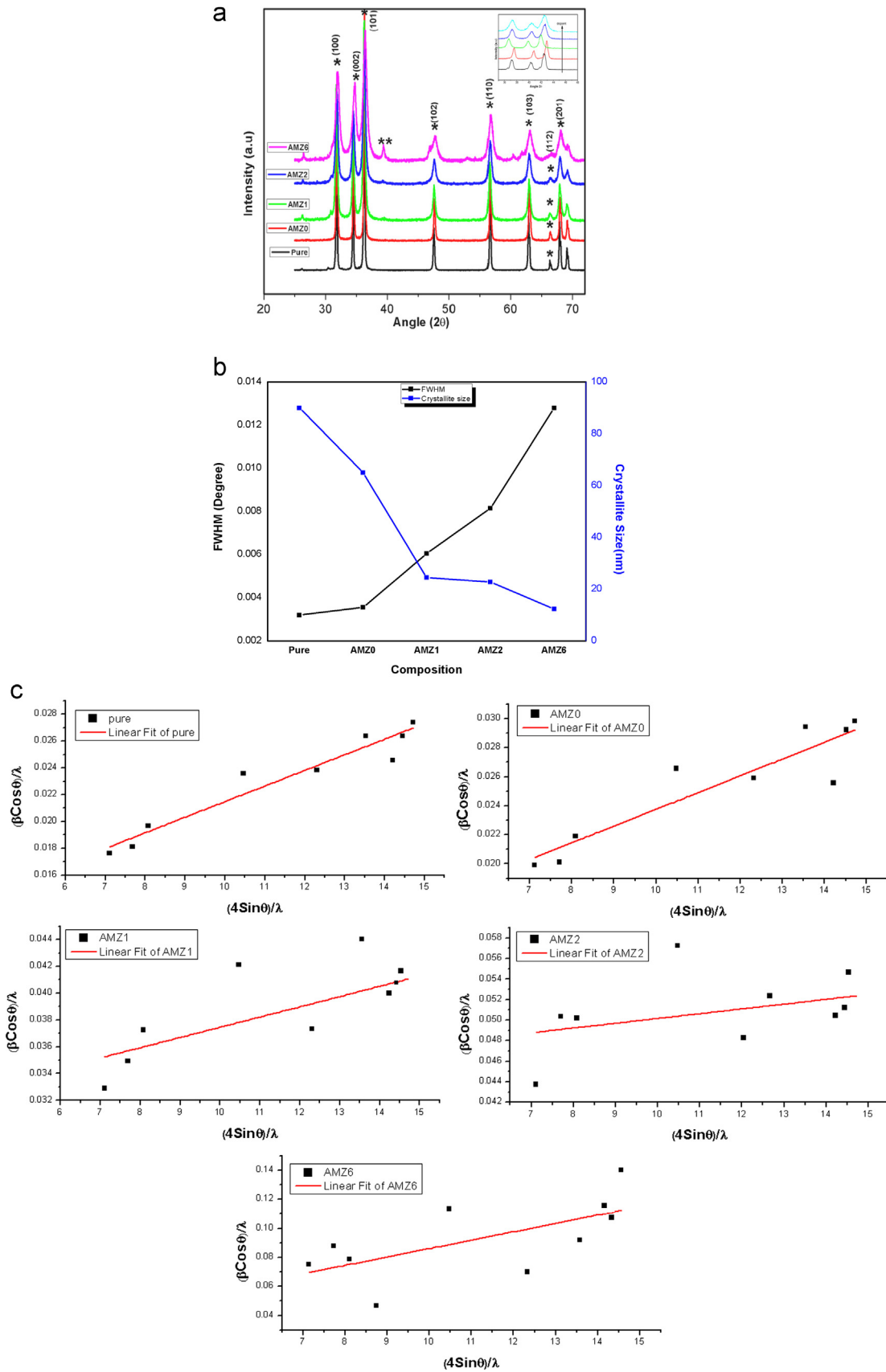


Fig. 1. (a). XRD patterns of undoped, Mg and Al co-doped ZnO nanoparticles. (b). Evaluation of the FWHM and Grain size with composition.

Table 1
The average crystallite sizes and the bond lengths of Mg and Al co-doped ZnO nanoparticles.

Sample	Crystallite size (nm)		Stain(ϵ)	Bond length (D) (Å)
	Scherrer's formula	W–H plot		
Pure	45	101	0.00116	1.788
AMZ0	41	81	0.00115	1.785
AMZ1	24	33	0.00076	1.788
AMZ2	17	21	0.00046	1.787
AMZ6	11	19	0.00357	1.782

length moderately increased, with further increase of Al concentrations at $x=0.02$ and 0.06 mol% (for AMZ2 and AMZ6), it observed to be decreased. Yao et al. assigned the changes in the bond length due to the residual stresses produced by substitution of Al ions into Zn ion lattice sites or redundant incorporation of Al ions into the crystal lattice interstitial sites [30]. The optical properties of the ZnO depend closely on the microstructures of the materials, including crystallite size, orientation, morphology, defects and lattice strain etc. [31]. W–H analysis is used to evaluate the strain induced in the samples due to Al and Mg co-doping. The average crystallite size and strain in nanoparticles were calculated from the spectral line shape using Williamson–Hall (W–H) plot using the following equation [22]:

$$\frac{\beta \cos \theta}{\lambda} = \frac{0.9}{d} + \frac{4\epsilon \sin \theta}{\lambda}$$

where β is the full width at half-maximum, ϵ is the lattice strain, θ is the Bragg angle, d is the average crystallite size and λ is the wavelength of X-rays. A plot drawn between $(\beta \cos \theta)/\lambda$ and $(4 \sin \theta)/\lambda$ gave rise to a straight line graph with a positive intercept as shown in Fig. 1(c). The strain is calculated from the slope of the linear fit and the y-intercept gives the inverse crystallite size. The crystallite sizes calculated from W–H plots for Pure, AMZ0, AMZ1, AMZ2 and AMZ6 are 102, 81, 33, 21 and 12 nm respectively. These results followed the same trend as in the case of crystallite sizes calculated from Scherrer's formula. It is observed from the W–H analysis that, the induced strain decreased with increase of Al doping concentrations while keeping the Mg content constant in ZnO.

3.2. FE-SEM

Microstructural characterization of synthesized samples was studied by FE-SEM. For morphological studies, gold coating is provided on the powder sample placed over a carbon tape. Fig. 2(a) depicts the FE-SEM images of the pristine ZnO, Mg and Al co-doped ZnO. It is clear from these images that, pristine ZnO exhibited the hexagonal morphology. With Mg and Al co-doping, the grain sizes decreased and the shape changes to spherical morphology. The compositions of pure ZnO and AMZ nanoparticles were determined through EDS, which showed the presence of Al, Mg, Zn, and O as elementary components. The typical EDS spectra of pure ZnO and AMZO nanoparticles are shown in Fig. 2(b). From Fig. 2(a) the particle size of AMZ1 is smaller than AMZ2 can

be explained on the basis of the Zener pinning effect [32]. The decrease in the crystallite size or particle size was explained with the help of the following equations:

$$F_{max} = \pi r_p \gamma_b$$

where γ_b is the grain boundary energy and r_p is the obstacle radius.

The retarding force per unit area F_r is given by:

$$F_r = \frac{3f_r \gamma_b}{2r_p}$$

and the average driving force F_d is given by:

$$F_d = \frac{\alpha \gamma_b}{r}$$

where r is the particle radius, γ_b is the grain boundary energy and α is a geometrical constant.

Therefore, the presence of a greater retarding force produced a greater inhibition for the growth of particles. With the doping of Al ($x=0.01$ mole% (AMZ1)), the retarding force could increase with the increase of number of obstacles per unit volume adhered on the ZnO surface. Consequently, there is decrease in the particle size of ZnO nanocrystals. With further increase of Al doping concentration to $x=0.02$ (AMZ2), the efficiency of the pinning reduces as the particles coarsen, giving rise to a change in the ratio of f_r/r_p as a result of increase in r_p . Hence, the pinning under certain conditions may lead to the particle growth. Hence, the growth in the particle size for AMZ2 sample may be due to the coarsening of the doping metal. This could be the reason for the shape changes occurred in morphology with increase of Al doping in ZnO.

3.3. Raman spectroscopy

To investigate the vibrational properties of the ZnO nanostructures, Raman scattering measurement was performed at room temperature. Raman is very sensitive and non-destructive tool for investigating semiconductor nanostructures. According to the group theory, wurtzite ZnO belongs to the space group c_{6v}^4 , with two formula units per primitive cell and therefore, there are the Raman-active phonon modes E_2 (low), E_2 (high), A_1 longitudinal optical (LO), A_1 transverse optical (TO), E_1 (LO), and E_1 (TO). Only two B_1 modes are Raman and infrared inactive [33]. E_2 (high) is associated with oxygen atoms and E_2 (low) is associated with Zn sublattice. According to the well-known Raman selection rules, only the E_2 modes and the A_1 (LO) mode were expected to emerge, and the other modes were forbidden [34]. The typical Raman spectra of Mg and Al co-doped ZnO nanoparticles are shown in Fig. 3(a). Several peaks at 331, 382, 410, 436, and 564 cm^{-1} were observed, which were attributed to optical phonons of ZnO. The intense and fairly narrow peak at 436 cm^{-1} correspond to a non-polar optical phonon E_2 (high) of wurtzite ZnO while the 331 cm^{-1} is assigned to the second-order Raman spectrum arising from zone boundary phonons of the hexagonal ZnO [35]. The strong E_2 (high) is a characteristic of the wurtzite lattice and indicates good crystallinity. With increase of the doping concentrations, E_2 (high) phonon frequency shifted

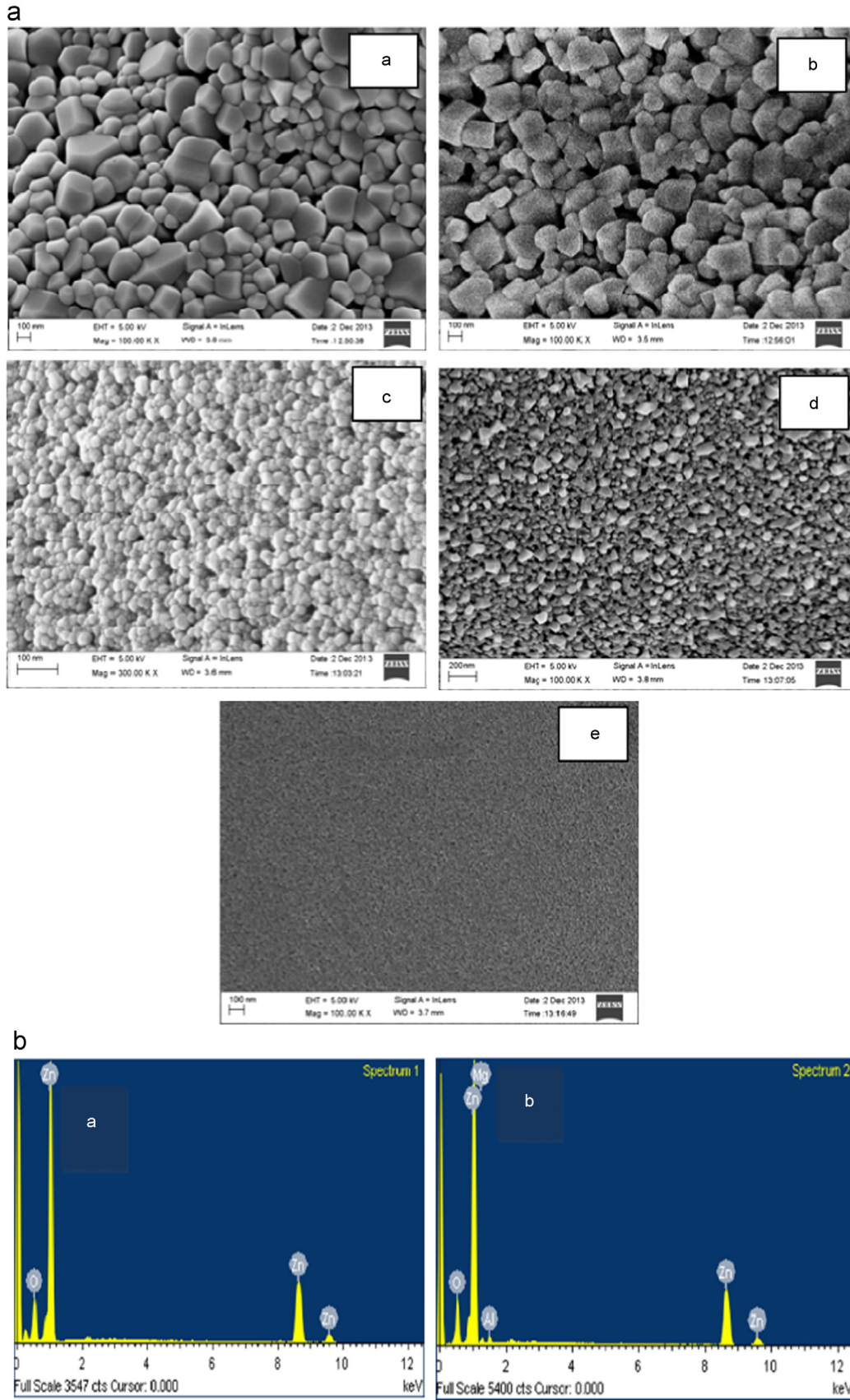


Fig. 2. (a). FE-SEM images of a) undoped ZnO b) AMZ0 c) AMZ1 d) AMZ2 and e) AMZ6, (b). EDAX spectrum of a) undoped b) Mg and Al co-doped ZnO nanoparticles.

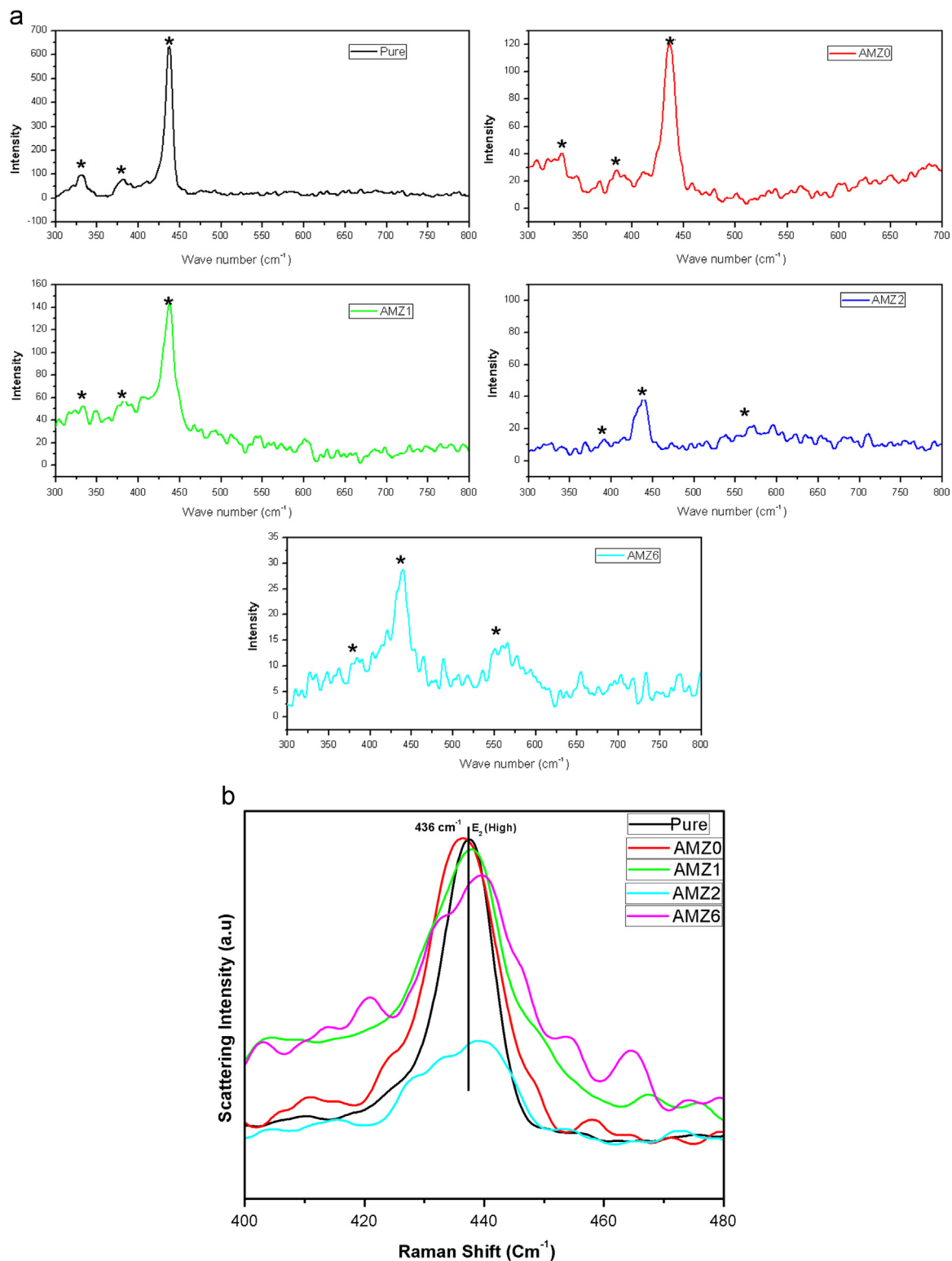


Fig. 3. (a). Raman spectra of pristine ZnO and Mg and Al co-doped ZnO. (b). Raman shift with increase of doping concentrations of Mg and Al in ZnO nanoparticles.

from 436 to 439 cm⁻¹ as shown in Fig. 3(b). E₂ (high) phonon frequency is red-shifted by 3.0 cm⁻¹ compared to that of the undoped ZnO, which showed a strong E₂ mode at 439 cm⁻¹. The origin of E₂ (high) peak shift in ZnO nanoparticles may be attributed to optical phonon confinement effects or the

presence of intrinsic defects on the nanoparticles [36]. In addition to this, another peak was observed at 564 cm⁻¹ with increase of doping concentrations and is attributed to the A₁ (LO) mode of the hexagonal ZnO. These additional modes seem to be related to the dopants which may be used as an

indication of their incorporation. Further the intensity of 436 cm^{-1} peak decreased for AMZ2 and AMZ6 concentrations which corroborated to XRD results.

3.4. UV–vis

The typical absorption spectra of the samples are shown in Fig. 4(a). A practical method is to equate E_g with the wavelength at which the absorption is 50% of the excitonic peak (shoulder), called $\lambda_{1/2}$ [37,3]. This is schematically shown in Fig. 4(b), for one sample and the same carried out for rest of the samples. Therefore energy $E(\lambda_{1/2})$ of pure ZnO is 3.20 eV and for other doped samples AMZ0, AMZ1, AMZ2 and AMZ6, it is 3.311 eV, 3.22 eV, 3.19 eV and 3.20 eV respectively. It is clear that with Mg doping (without Al doping), the band gap was increased to 3.311 eV from 3.20 eV, but with incorporation of Al concentration, the band gap decreased. However, by keeping Mg doping constant in ZnO and increasing Al concentration up to AMZ6 ($x=0.06$) resulted the band gap to attain as it was for pure ZnO sample. The particle sizes were estimated using effective mass approximation by converting the energy corresponding to the exciton absorption peak using the following expression [22]:

$$E = E_g + h^2 \pi^2 \left(\frac{1}{m_e} + \frac{1}{m_h} \right) - \left(\frac{1.8e^2}{4\pi\epsilon'\epsilon_0 R} \right) + \text{smaller term}$$

where E is the band gap of the synthesized particle, E_g is the bulk energy of ZnO (3.37 eV), R is the radius of the particle, m_e is the effective mass of the electron ($0.28m_0$), m_h is the effective mass of the hole ($0.49m_0$), ϵ' is the dielectric constant of the material (9.1), ϵ_0 is the permittivity of the free space, h is Planck's constant. The obtained values of the particle radius from the mass approximation is 5.24 nm, 2.99 nm, 4.26 nm, 5.24 nm, 4.52 nm for pure, AMZ0, AMZ1, AMZ2, AMZ6 respectively.

3.5. Photoluminescence analysis

Photoluminescence (PL) and optical absorption measurements are also extremely helpful for characterization of ZnO material. The optical band gap of the material as well as the possible radiative and non-radiative centers can be understood from these techniques [38,39]. The photoluminescence (PL) spectrum of ZnO is normally composed of two parts: excitonic near band edge emission with energy around the band gap of ZnO and defect related deep level emission in the visible range [40,41]. In addition to UV excitonic emission peak, ZnO in general exhibits visible luminescence at different emission wavelengths due to intrinsic or extrinsic defects. The origin of these emissions, especially the green emission has been controversial [42]. This is due to the variety of synthesis procedures that have been used in the preparation of ZnO nanoparticles and also due to the complexity in its micro-structure. The room temperature PL spectrum of all the samples is shown in Fig. 5. From the PL spectrum, a sharp UV emission positioned at 395 nm is observed for all the samples and the most familiar green emission of ZnO was not

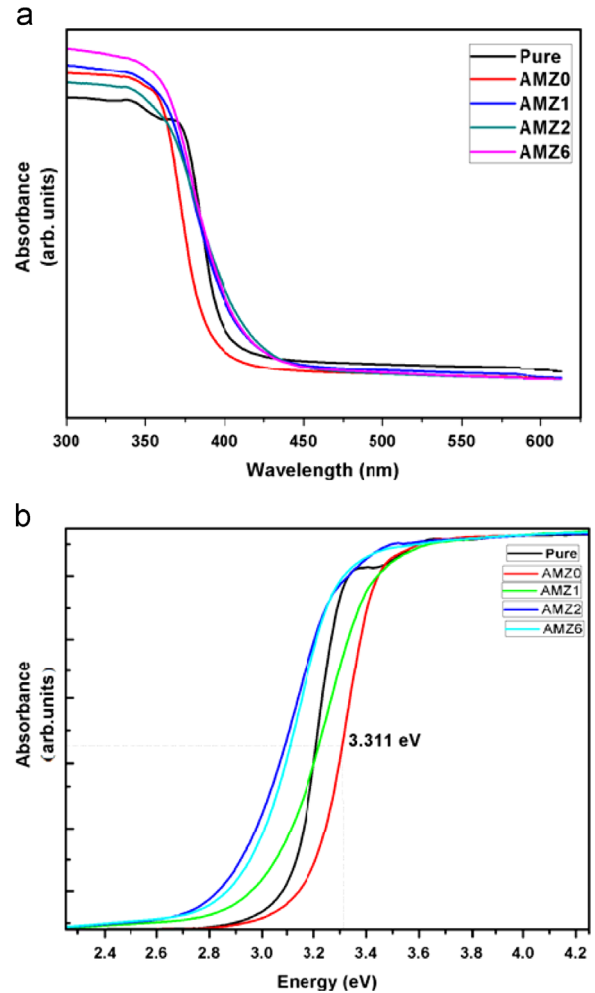


Fig. 4. (a). Absorption spectra of undoped and Mg, Al co-doped ZnO nanoparticles. (b). Absorption profile of ZnO and Mg, Al co-doped ZnO nanoparticles.

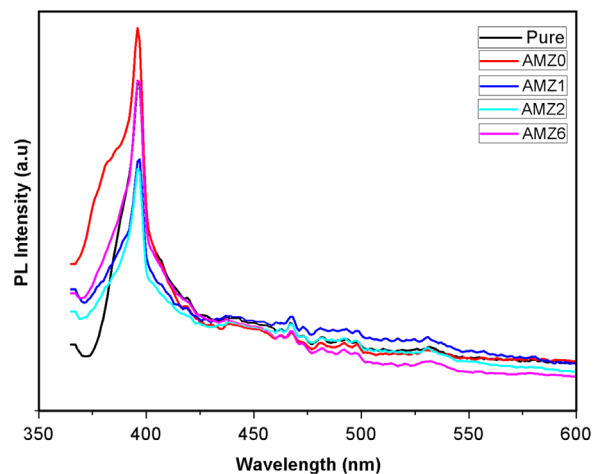


Fig. 5. PL spectra of ZnO nanoparticles at room temperature.

observed for these samples. In general, the origin of UV emission in ZnO was attributed to four factors. They are (i) direct transition from conduction band (C.B) to valence band

(V.B); (ii) transition of zinc interstitial (Zn_i) defect level to V.B; (iii) transition from the C.B to zinc vacancy (V_{Zn}) which is a result of blue–green emission of the material; and (iv) transition from Zn_i to V_{Zn} [43]. The emission peak positioned at 395 nm is originated from the electron transition from the localized energy level slightly below conduction band to the valence band. Along with this, in case of Mg doped sample (AMZ0), there is a kink positioned at 387 nm. This may be attributed to the near band edge emission. The intensity of the Mg doped ZnO peak was observed to be higher than undoped sample. Further with Al co-doping in to ZnO, the peaks got broadened and there is a decrease in the intensity of the peaks. Further, the UV emission is also dependent on the grain size and crystal orientation [44]. In the present study, the grain size as well as the intensities of the diffraction peaks decreased with increasing doping concentrations. Matsumoto et al. correlated the intensity of PL with grain size effects by taking into account radiative and non-radiative recombination trapping rates occurring in ZnO grain boundaries [45]. With decreasing crystallite sizes, the surface-to-volume ratio becomes larger. Due to this, smaller grains have larger non-radiative relaxation rates from the surface states. This non-radiative relaxation process occurring in the surface states decreased with Mg and Al co-doping and for AMZ6 it was observed to be increased. This increase in the non-radiative transitions gives indication of decrease in the crystallite sizes.

4. Conclusions

From XRD analysis, the hexagonal wurtzite structure of ZnO was confirmed, and no other impurity phase corresponding to the dopants was found. It infers that the dopants are within the solid solubility limit. Moreover, the observed peak shift of the diffraction angle and the dramatic decrease of intensity with increase in the Al dopant concentrations suggest that, the dopant ions were uniformly substituted into the Zn sites or interstitial sites in ZnO lattice. The observed width broadening factor has been assigned to the decrease of crystal size. The crystallite sizes were estimated using Scherrer's formula and followed the same trend as observed in (i) FE-SEM morphology studies (ii) and also for the particle sizes estimated from absorption spectra based on effective mass approximation. Raman spectroscopic investigations showed the characteristic peak of wurtzite ZnO at 436 cm^{-1} corresponds to the E_2 (high) mode. The origin of E_2 (high) peak shift in ZnO nanoparticles was attributed to optical phonon confinement effects or the presence of intrinsic defects on the nanoparticles. The energy or the band gap estimated from absorption data was increased for AMZ0 but with increase of Al co-doping it decreased. With Mg doping the intensity of the excitonic emission peak increased along with near band edge emission. Initially, the PL intensity was reduced with increasing Al co-doping, which corroborates the same results observed with grain size effects from FE-SEM study. The particle size or grain size dependence of the emission properties is thus correlated.

Acknowledgments

The authors are thankful to Dean, School of Physics, UoH, for providing FE-SEM facility and also to the FE-SEM operator Ms. Arundhathi for her help in taking the measurements. The authors express their gratitude to Dr. T. Ramakrishna Reddy, SVU, for his kind help in taking the Raman.

References

- [1] S.J Pearton, D.P. Norton, K. Ip, Y.W. Heo, T. Steiner, Recent progress in processing and properties of ZnO, *Prog. Mater. Sci.* 50 (2005) 293–340.
- [2] C. Klingshirn, ZnO: from basics towards applications, *Phys. Status Solidi (b)* 244 (2007) 3027–3073.
- [3] Meulenkamp Eric A., Synthesis and growth of ZnO nanoparticles, *J. Phys. Chem. B* 102 (1998) 5566–5572.
- [4] D.J. Cohen, K.C. Ruthe, S.A. Barnett, Transparent conducting $Zn_{1-x}Mg_xO$ (Al, In) thin films, *J. Appl. Phys.* 96 (2004) 459.
- [5] V Shelke, M.P. Bhole, D.S. Patil, Effect of open air annealing on spin coated aluminum doped ZnO nanostructure, *Mater. Chem. Phys.* 141 (2013) 81–88.
- [6] H Kim, C M Gilmore, J.S. Horwitz, A. Piqué, H. Murata, et al., Transparent conducting aluminum-doped zinc oxide thin films for organic light-emitting devices, *Appl. Phys. Lett.* 76 (2000) 259–261.
- [7] S Singh, P Thiyagarajan, K Mohan Kant, D Anita, S Thirupathiah, N Rama, Brajesh Tiwari, M Kottaisamy, M S Ramachandra Rao, Structure, microstructure and physical properties of ZnO based materials in various forms: bulk, thin film and nano, *J. Phys. D: Appl. Phys.* 40 (2007) 6312–6327.
- [8] D Fanga, Pei Yao, H Li, Influence of annealing temperature on the structural and optical properties of Mg–Al co-doped ZnO thin films prepared via sol–gel method, *Ceram. Int.* 40 (2014) 5873–5880.
- [9] Z.K. Heiba, L. Arda, M Bakr Mohamed, M.A. Al-Jalali, N. Dogan, Structural and magnetic properties of (Al/Mg) co-doped nano ZnO, *J. Supercond. Nov. Magn.* (2013), <http://dx.doi.org/10.1007/s10948-013-2174-8>.
- [10] J Xu, S. Shi, X. Zhang, Y Wang, M. Zhu, Lan Li, Structural and optical properties of (Al, K) co-doped ZnO thin films deposited by a sol–gel technique, *Mater. Sci. Semicond. Process.* 16 (2013) 732–737.
- [11] L. Arda, A. Gungör, D. Akcan, Synthesis, characterization and ESR studies of powder $Zn_{0.95-x}Mg_{0.05}Al_xO$ ($x=0, 0.01, 0.02, 0.05$ and 0.1) nanocrystals, *Solid State Commun.* 170 (2013) 14–18.
- [12] A Bikowski, K Ellmer, A comparative study of electronic and structural properties of polycrystalline and epitaxial magnetron-sputtered ZnO: Al and $Zn_{1-x}Mg_xO$: Al films-origin of the grain barrier traps, *J. Appl. Phys.* 114 (2013) 063709.
- [13] A Bandyopadhyay, S Modak, S. Acharya, A.K. Deb, P.K. Chakrabarti, Microstructural, magnetic and crystal field investigations of nanocrystalline Dy^{3+} doped zinc oxide, *Solid State Sci.* 12 (2010) 448–454.
- [14] M.R Vaezi, S.K Sadrezhaad, Nano powder synthesis of zinc oxide via solo chemical processing, *Mater. Des.* 28 (2007) 515–519.
- [15] A Aimable, M T Buscagli, V. Buscaglia, Paul Bowen, Polymer-assisted precipitation of ZnO nanoparticles with narrow particle size distribution, *J. Eur. Ceram. Soc.* 30 (2010) 591–598.
- [16] D. Dorranean, E Solati, L Dejam, Photoluminescence of ZnO nanoparticles generated by laser ablation in de ionized water, *Appl. Phys. A* 109 (2012) 307–314.
- [17] T.S. Ko, T.C. Lu, S. Yang, H.C. Hsu, C.P. Chu, H.F. Lin, et al., ZnO nanopowders fabricated by dc thermal plasma synthesis, *Mater. Sci. Eng. B* 134 (2006) 54–58.
- [18] K Okuyama, I. W Lenggono, Preparation of nanoparticles via spray route, *Chem. Eng. Sci.* 58 (2003) 537–547.
- [19] W.S. Chiu, P.S. Khiew, D. Isaa, M. Cloke, S. Radiman, R. Abd-Shukor, M.H. Abdullah, N.M. Huang, Synthesis of two-dimensional ZnO nano pellets by pyrolysis of zinc oleate, *Chem. Eng. J.* 142 (2008) 337–343.

- [20] Haixin Bai, X Liu, Green hydrothermal synthesis and photoluminescence property of ZnO₂ nanoparticles, *Mater. Lett.* 64 (2010) 341–343.
- [21] Mikrajuddin, F. Iskandar, K. Okuyama, F.G. Shi, Stable photoluminescence of zinc oxide quantum dots in silica nanoparticles matrix prepared by the combined sol–gel and spray drying method, *J. Appl. Phys.* 89 (2001) 6431.
- [22] A.N. Mallika, A.R. Reddy, K.S. Babu, Ch. Sujatha, K.V. Reddy, Structural and photoluminescence properties of Mg substituted ZnO nanoparticles, *Opt. Mater.* 36 (2014) 879–884.
- [23] Y. S Wang, P. John Thomas, P.O Brien, Optical properties of ZnO nanocrystals doped with Cd, Mg, Mn, and Fe ions, *J. Phys. Chem. B* 110 (2006) 21413.
- [24] Yow-Jon Lin, Chia-Lung Tsaia, Yu-Chih Tseng, Wei-Min Cho, et al., Effects of ultraviolet treatment on the optical and structural properties of ZnO nanoparticles, *Mater. Chem. Phys.* 130 (2011) 299–302.
- [25] Cullity BD. *Elements of X-ray diffraction*. Philippines: Addison-Wesley Publishing Company; 978.
- [26] R. Elilarassi, G. Chandrasekaran, Effect of annealing on structural and optical properties of zinc oxide films, *Mater. Chem. Phys.* 121 (2010) 378–384.
- [27] M.H. Mamat, M.Z. Sahdan, Z. Khusaimi, A. Zain Ahmed, S. Abdullah, M. Rusop, Influence of doping concentrations on the aluminum doped zinc oxide thin films properties for ultraviolet photoconductive sensor applications, *Opt. Mater.* 32 (2010) 696–699.
- [28] X.S Wang, Z.C Wu, J. webz, G. liu, Ferroelectric and dielectric properties of Li-doped ZnO thin films prepared by pulsed laser deposition, *Appl. Phys. A* 77 (2003) 561–565.
- [29] F.K. Shan, B.I. Kim, G.X. Liu, Z.F. Liu, J.Y. Sohn, W.J. Lee, B.C. Shin, Y.S. Yu, Blue shift of near band edge emission in Mg doped ZnO thin films and aging, *J. Appl. Phys.* 95 (2004) 4772–4775.
- [30] D Fang, K Lin, Pei Yao, Tao Xue, Can Cui, Xiaoping Chen, Huijun Li, Influence of Al doping on structural and optical properties of Mg–Al co-doped ZnO thin films prepared by sol–gel method, *J. Alloy. Compd.* 589 (2014) 346–352.
- [31] P.K. Giri, S. Bhattacharyya Dilip, K. Singh, R. Kesavamoorthy, B. K. Panigrahi, Correlation between microstructure and optical properties of ZnO nanoparticles synthesized by ball milling, *J. Appl. Phys.* 102 (2007) 093515.
- [32] S Suwanboon, P Amornpitoksuk, A Sukolrat, Dependence of optical properties on doping metal, crystallite size and defect concentration of M-doped ZnO nanopowders (M=Al, Mg, Ti), *Ceram. Int.* 37 (2011) 1359–1365.
- [33] Jiandong Ye, S Gu, Shunmin Zhu, Tong Chen, Wei Liu, F Qin, L Hu, R Zhang, Yi Shi, Youdou Zheng, Raman and photoluminescence of ZnO films deposited on Si (111) using low-pressure metalorganic chemical vapor deposition, *J. Vac. Sci. Technol. A.* 21 (2003) 979.
- [34] T.C. Damen, S.P.S. Porto, B. Tell, Raman effect in zinc oxide, *Phys. Rev.* 142 (1966) 570–574.
- [35] A.J. Reddy, M.K. Kokila, H. Nagabhushana, J.L. Rao, C. Shivakumara, B.M. Nagabhushan, R.P.S. Chakradhar, Combustion synthesis, characterization and Raman studies of ZnO nanopowders, *Spectrochim. Acta A* 81 (2011) 53–58.
- [36] R D Yang, S. Tripathy, Yuntao Li, H-J Sue, Photoluminescence and micro-Raman scattering in ZnO nanoparticles: the influence of acetate adsorption, *Chem. Phys. Lett.* 411 (2005) 150–154.
- [37] A Sharma, B.P Singh, S Dhar, A Gondorf, M. Spasova, Effect of surface groups on the luminescence property of ZnO nanoparticles synthesized by sol-gel route, *Surf. Sci.* 606 (2012) L13–L17.
- [38] K Vanheusden, C.H Seager, W.L. Warren, D.R. Tallant, J.A. Voigt, Correlation between photoluminescence and oxygen vacancies in ZnO phosphors, *Appl. Phys. Lett.* 68 (1996) 403.
- [39] V. Srikant, D.R. Clarke, Optical absorption edge of ZnO thin films: the effect of substrate, *J. Appl. Phys.* 81 (1997) 6357.
- [40] Y.G. Wang, S.P. Lau, H.W. Lee, S.F. Yu, B.K. Tay, et al., Photoluminescence study of ZnO films prepared by thermal oxidation of Zn metallic films in air, *J. Appl. Phys.* 94 (2003) 354.
- [41] A.B. Djuriscic, Y.H. Leung, Optical properties of ZnO nano structures, *Small* 2 (2006) 944–961.
- [42] A.B Djuriscic, Y.H Leung, K.H. Tam, L. Ding, W.K. Ge, et al., Green, yellow and orange defect emission from ZnO nanostructures: influence of excitation wavelength, *Appl. Phys. Lett.* 88 (2006) 103107.
- [43] T. Prasada Rao, G.K. Goswami, K.K. Nanda, Detailed understanding of the excitation-intensity dependent photoluminescence of ZnO materials: role of defects, *J. Appl. Phys.* 115 (2014) 213513.
- [44] P.T. Hsieh, Y.C. Chena, K.S. Kao, M.S. Lee, C.C. Cheng, The ultraviolet emission mechanism of ZnO thin film fabricated by sol–gel technology, *J. Eur. Ceram. Soc.* 27 (2007) 3815–3818.
- [45] T Matsumoto, Zhukov Hiroyuki Kato, K Miyamoto, M Sano, A Evgeniy, Zhukov, et al., Correlation between grain size and optical properties in zinc oxide thin films, *Appl. Phys. Lett.* 81 (2002) 1231.